JACS
JOURNAL OF THE AMERICAN CHEMICAL SOCIETY

Article

pubs.acs.org/JACS

A Direct Biocombinatorial Strategy toward Next Generation, Mussel-Glue Inspired Saltwater Adhesives

Patrick Wilke,[†] Nicolas Helfricht,[‡] Andreas Mark,[‡] Georg Papastavrou,[‡] Damien Faivre,[§] and Hans G. Börner*[,†]

[†]Department of Chemistry, Laboratory for Organic Synthesis of Functional Systems, Humboldt-Universität zu Berlin, D-12489 Berlin, Germany

[‡]Physical Chemistry II, University of Bayreuth, D-95440 Bayreuth, Germany

[§]Department of Biomaterials, Max Planck Institute of Colloids and Interfaces, Science Park Golm, D-14424 Potsdam, Germany

Supporting Information

ABSTRACT: Biological materials exhibit remarkable, purpose-adapted properties that provide a source of inspiration for designing new materials to meet the requirements of future applications. For instance, marine mussels are able to attach to a broad spectrum of hard surfaces under hostile conditions. Controlling wet-adhesion of synthetic macromolecules by analogue processes promises to strongly impact materials sciences by offering advanced coatings, adhesives, and glues. The *de novo* design of macromolecules to mimic complex aspects of mussel adhesion still constitutes a challenge. Phage display allows material scientists to design specifically interacting molecules with tailored affinity to material surfaces. Here, we report on the integration of enzymatic processing steps into phage display biopanning to expand the biocombinatorial procedure and enable the direct selection of enzymatically activable peptide adhesion domains. Adsorption isotherms and single molecule force spectroscopy show that those *de novo* peptides mimic complex aspects of bioadhesion, such as enzymatic activation (by tyrosinase), the switchability from weak to strong binders, and adsorption under hostile saltwater conditions. Furthermore, peptide-poly(ethylene oxide) conjugates are synthesized to generate protective coatings, which possess anti-fouling properties and suppress irreversible interactions with blood-plasma protein cocktails. The extended phage display procedure provides a generic way to non-natural peptide adhesion domains, which not only mimic nature but also improve biological sequence sections extractable from mussel-glue proteins. The *de novo* peptides manage to combine several tasks in a minimal 12-mer sequence and thus pave the way to overcome major challenges of technical wet glues.

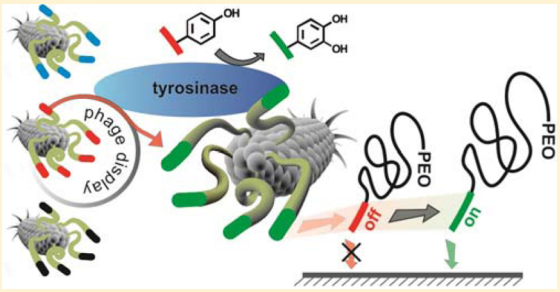

INTRODUCTION

Marine mussels adhere rapidly in hostile environments onto practically any hard surface and in many aspects their adhesive properties still outperform state of the art wet glues.[1,2] Tremendous efforts have been spent to understand and mimic the byssal adhesive system to realize bioinspired coatings or glues.[3−7] Waite et al. described the underlying biochemistry as a concerted process in which several purpose-adapted proteins are expressed, enzymatically processed, and excreted to form the adhesive byssus.[3,8−10] Within those regulated processes the enzymatic oxidation of tyrosine residues in adhesive protein precursors has been identified as one of the key steps.[5,11,12] On the one hand, the generated L-3,4-dihydroxyphenylalanine (L-dopa) residues contribute to cohesion, building chemical cross-links between adhesive proteins.[10,13] On the other hand, L-dopa plays a dominant role in adhesion, generating effective interfaces to various surfaces.[4,7] Identification of the importance of L-dopa residues led to mussel-glue inspired polymers that mimic certain aspects of the mussel adhesives. The first segmented copolymers containing L-dopa were realized in a pioneering study by Yamamoto et al. in 1978.[14] Messersmith et al. significantly expanded the scope of applications and exploited L-dopa-containing polymers for materials and biomedical sciences.[1,15,16] For instance, poly(ethylene oxide)-*block*-(L-dopa)$_{1-3}$ (PEO-(L-dopa)$_{1-3}$) led to anti-fouling coatings, and (PEO-L-dopa)$_4$ star polymers formed hydrogels with accurately adjustable mechanical properties.[17,18] Deming et al. accessed poly(L-dopa-*co*-L-Lys) and demonstrated the utilization of chemical or enzymatic oxidation to remarkably improve cohesion in those adhesives.[12,19] More recently, Börner et al. described the use of tyrosinase to activate adhesion properties of bioconjugates composed of PEO and a precursor segment of the mussel foot protein 1 of *Mytilus edulis* (mefp-1).[20]

However, mefp-1 serves in nature only as a protective coating of the mussel byssus. Hence, the enzyme activated mefp-1-*block*-PEO failed to adhere efficiently under seawater

Received: June 4, 2014
Published: August 18, 2014

   dx.doi.org/10.1021/ja505413e | J. Am. Chem. Soc. 2014, 136, 12667−12674

conditions. This failure imposed the need for finding more suitable sequences in order to improve bioinspired, enzyme-activated coatings and obtain synthetic sequence models to better understand and mimic bioadhesive processes.

Biocombinatorial approaches, such as phage display, represent a widely exploited strategy to select peptides or proteins that exhibit highly specific affinity to substrates.[21] The resulting methodology was applied to various biological entities, and more recently the exciting opportunities for materials sciences were explored.[22] Thereby, peptides have been selected, which discriminate between highly related semiconductor surfaces,[23] differentiate poly(methyl methacrylate)s with different tactility,[24] control biomimetic crystallization,[25,26] or bind strongly to biomedical relevant material surfaces.[27,28] However, these established biopanning methods are not applicable to directly screen for mussel inspired adhesives as the sequences of interest have to meet additional requirements apart from just specific interactions to a target surface (cf. Figure 1b).

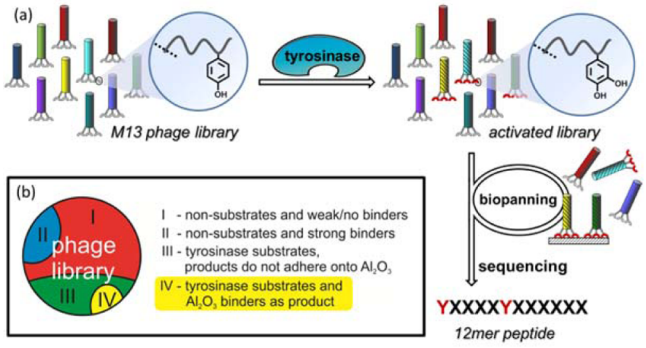

Figure 1. Illustration of the advanced phage display cycle (a) consisting of a tyrosinase processing of the entire library (top) and biopanning under harsh conditions to select binding phages to be sequenced for bioconjugate synthesis (right) and the objective to select appropriate peptide sequences with desired property profiles from the sequential space spanned by the phage library (b).

Here, we describe an advanced biocombinatoric screening strategy that enables the selection of enzyme triggered adhesive peptides for construction aluminum. The common biopanning was expanded with a tyrosinase processing step leading to a generic procedure, which enables the direct selection of peptides having excellent substrate properties for the enzyme of interest (e.g., tyrosinase). Moreover, the peptides should in the non-activated state show weak or no binding to surfaces of interest. Activation of the peptide substrate by tyrosinase should significantly increase the adhesive properties leading to highly adhesive peptides, which even allow generating stable coatings under saltwater conditions.

METHODS

Peptide/Conjugate Activation. Enzymatic activation kinetics of peptides and peptide–polymer conjugates were carried out using 100 units of tyrosinase and 0.29 μmol substrate in a final volume of 1 mL incubated at 25 °C (protocol modified from procedures described by Waite et al.).[29] Peptide and conjugates (0.29 μmol/mL) were dissolved in potassium phosphate buffer (17 mM, pH 6.5). Subsequently, the solution for activation of the peptides/conjugates was prepared by mixing 33 μL of 2.2 mM (for UV kinetics; activation to quinone) ascorbic acid or 220 mM (for QCM measurements, activation to L-dopa) sodium ascorbate and 100 units of tyrosinase in 50 mM potassium phosphate buffer (pH 6.5) with 10 μL of 0.2 mM L-dopa in a separate tube. To start the oxidation, this solution was transferred to the peptide or conjugate. Kinetic plots were obtained for 15 h. Peptide conversion was evaluated via MALDI-TOF-MS.

UV–vis Kinetics. UV–vis spectroscopy was carried out on a Varian Cary 100 Bio UV–vis spectrophotometer (Agilent Technologies) with a Varian Cary temperature controller unit using quartz cuvettes (enzymatic assay). Peptide/Conjugate activation was monitored on a EonC Microplate Specralphotometer (BioTec, Germany) using UV 96-well plates (Fisher Scientific, Germany). Kinetic plots were obtained at 25 °C reading at 280 nm.

Quartz Crystal Microbalance. Quartz crystal microbalance measurements were conducted on a Q-sense E1 single-sensor QCM-D module (Q-Sense, Sweden) with QE 401 electronic unit and equipped with a multichannel pump (IPC Ismatec SA, Switzerland). Piezoelectric sensor crystals coated with 50 nm aluminum oxide (Q-Sense, Sweden) were cleaned in an ultrasonic bath with 2% Helmanex in Milli-Q-water for 15 min and ethanol for 10 min prior to use. Subsequently, sensors were thoroughly washed Milli-Q-water and dried under compressed air flow. Finally, crystals were cleaned in a ZEPTO plasma cleaner (diener electronics, Germany) for 3 min at 75 W by air plasma. Immediately afterward, the sensors were mounted into the flow chamber and incubated with buffer using a flow rate of 100 μL/min until the frequency signals were constant (1–3 h). Subsequently, samples with a concentration of 50 mg/mL in buffer were pumped into the flow chamber, and signals were again monitored until being constant. Following measurements were conducted with 0.8 mM potassium phosphate buffer (pH 6.5), 599 mM NaCl, 10 mg/mL bovine serum albumin (BSA) as well as fetal bovine serum and human serum. Experiments were performed at 22 °C (unless stated otherwise) and overtones 3, 5, 7, 9, 11, and 13 were recorded. If not stated otherwise, the third overtones of all experiments were used for evaluation of the frequency shift.

Single Molecule Force Spectroscopy. The single molecule force spectroscopy was performed with a MFP-Plus equipped with an ARC2-controller and a standalone base (Asylum Research, Santa Barbara, CA). The instrument was placed on an active vibration isolation and in an acoustic shielding. In order to detect the detachment of single peptides from the aluminum oxide surface the peptide has to be covalently coupled to the tip of an AFM cantilever by means of a PEO-spacer (cf. SI). Typically, the single molecule experiments have been performed with a ramp size of about 250 nm, which is significantly larger than the length of the PEO spacer. The single force curves were acquired at a cantilever velocity of about 100 nm/s and a data acquisition rate of 50000 kHz. In order to increase the probability of peptide binding, a dwell time of 4 s has been applied during which the probe remains in contact with the sample surface. For each peptide-PEO-modified cantilever at least 1000 curves at 5 different positions have been acquired. All measurements were performed in 0.8 mM potassium phosphate buffer (pH 6.5, without addition of ascorbic acid). The pH has been controlled directly before the measurements. As sample the same sensors as used for the QCM measurements have been used. The spring constant of the cantilevers has been determined by the thermal noise method. For the conversion of the raw data a program based on standard algorithms written in IGOR Pro (Wavemetrics) has been used (cf. SI).

RESULTS AND DISCUSSION

The selection of mussel inspired adhesion domains via phage display methodologies intends to find peptides that fulfill complex requirements, making the adaptation of biopanning protocols essential (cf. Figure 1). The selected sequences should be (i) effective enzyme substrates and (ii) possess in the non-activated state weak or no adhesive properties to the material surface of interest. From the sequential space of peptides that meet these requirements, the method has to furthermore discriminate sequence populations that (iii) will not adhere to the surface of interest after enzymatic processing.

dx.doi.org/10.1021/ja505413e | J. Am. Chem. Soc. 2014, 136, 12667–12674

Hence, a strategy was chosen that enables the selection of those sequences, for which adhesion will occur only after enzymatic activation (cf. Figure 1). A proof of principle was demonstrated by using mushroom tyrosinase as an inexpensive enzyme analogue of the oxidase from marine mussels, which process L-tyrosine residues into L-dopa. Aluminum (more accurately the alumina passivation layer of aluminum oxide) was chosen as one important lightweight construction material, where gluing and surface modification would be of interest.

The established protocols of biopanning had to be modified and accompanied by an enzymatic activation step. Figure 1 summarizes the adapted phage display and biopanning cycle. In contrast to common procedures, where phage−surface interactions are carefully equilibrated by long incubation times under mild conditions, the applied non-equilibrium biopanning uses comparatively harsh conditions (pH 4) and short contact times (1 s) to suppress the selection of non-activated strong binders. To select peptide sequences that exhibit strong adherence after being oxidized by tyrosinase, the entire phage library was enzymatically processed prior to the panning procedure. For that purpose, the phage pool was treated with tyrosinase (100 u/mL) and 0.1 mM ascorbic acid in potassium phosphate buffer (pH 6.5) for 3 h to oxidize the available tyrosine (Tyr) substrates. The reaction time was chosen as a compromise to activate the phage library most effectively but prevent activation of rather poor, slowly activable substrates. Noteworthy, short reaction times (1 h) did not result in significant enrichment of tyrosine in the selected binding domains (data not shown). After enzyme removal, the "activated" library was incubated with an Al_2O_3 surface in citrate buffer at pH 4 (10 repetitions of approximately 1 s). Rigorous washing steps at pH 2.2 with glycine hydrochloride buffer elute most of the non-activated phages from the Al_2O_3 surface as shown by reference experiments with the initial non-activated phage library (cf. SI). Final elution of residual strong binding phages was realized by trypsinization. The eluted subset of phages was isolated, amplified, and used for a second round, repeating the panning with increased selection pressure for a total of three rounds. Subsequently, a total of 44 phages were selected and sequenced. The resulting peptide sequences are summarized in Figure 2 (for the full sequence set cf. SI).

A successful selection procedure was suggested by the obvious increase of L-tyrosine residues in the selected set of peptides (cf. Figure 2). The total occurrence frequency for tyrosine over all found sequences was about 13%, which comprises an accumulation with respect to 3.9% in the initial library (cf. SI). Roughly 80% of the analyzed peptides showed one or more tyrosine residues. From 44 sequenced phages, a total number of 30 sequences contained tyrosine, and only 8 peptides were tyrosine-free (6 phages did not show an insert). Furthermore, 5 different sequences contained 2−3 tyrosine residues. It has to be pointed out that phage display screening on aluminum substrates under standard conditions does not lead to an accumulation of tyrosine.[30] Generally, higher L-dopa content exhibits stronger adhesion. Nonetheless, mussel adhesive proteins contain up to approximately 30 mol% L-dopa.[2] It also has been shown that incorporation of L-dopa in for instance polystyrene polymers only showed stronger adhesion up to 33 mol%.[31] Therefore, a 12-mer peptide theoretically could contain up to 4 L-dopa moieties. For the present study, tyrosinase substrate characteristics of each tyrosine residue also are of high importance. Hence, 12-mer

(a)

abbrev.	sequence	occurance
	YANATIYNKIKR	1
Pep1	YPATYYGMRSPS	2
Pep2	YHPNGMNPYTKA	21
Pep3	HSYSGWSPYRSG	2
	RSAVIRYQTASY	1
	YNFQHFNRFLTG	1
Pep4	HTEHHDKHSHRA	3
	VSLPKNFHSNPR	1
	TMLTHNPKPVKH	1
	without insert	6

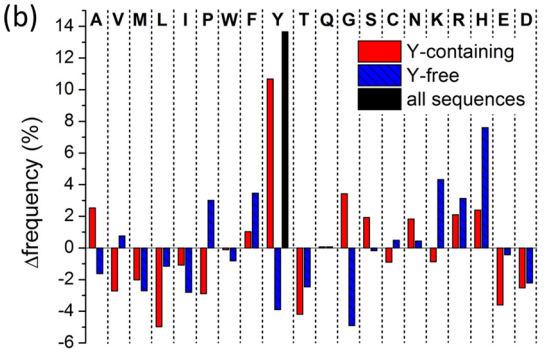

Figure 2. Excerpt from the 12-mer peptide adhesion domains selected from third round of enzyme activated phage display screening indicating an accumulation of tyrosine containing peptides (a) and in-depth analysis of the amino acid occurrence in the selected sequences showing the discrimination or enrichment of residues with respect to the occurrence in the initial phage library (b), statistics of tyrosine-containing peptides (red) and tyrosine-free peptides (blue) counted every sequence once and tyrosine content over all found sequences (black).

peptide sequences containing 2−3 tyrosine residues seem to constitute the best compromise out of activation and binding.

Global sequence analysis of the tyrosine-containing peptides indicated a preference for N-terminal tyrosine residues. Out of the eight different enzymatically processable peptides, five show multiple tyrosine (Tyr) residues. Usually, polar amino acids populate the direct neighbor positions next to tyrosine, but further preferences of amino acids for certain sequence positions were not obvious. Figure 2B summarizes the in-depth analysis of amino acid frequencies of residues that could be found in the selected sequences compared to the frequencies in the initial library. Counting every sequence only once and analyzing the subset of tyrosine-containing peptides, both acidic amino acids (E, D) and hydrophobic residues (V, M, L, P) obviously seem to be suppressed. Potentially the latter could be explained by lower substrate characteristics of tyrosine flanked by hydrophobic residues. Only minor deviation is shown for the majority of polar amino acids. Asparagine and serine are slightly enriched, whereas threonine is diminished. This was surprising, as previous reports of phage display on aluminum resulted in a dominance of hydroxyl group carrying amino acids, predominantly serine.[30] Nonetheless, besides tyrosine PeP_1 also contains two serine residues and one threonine, while Pep_3 bears even four serines. Basic amino acids with soft cations like arginine and histidine are slightly favored, reflecting the known interactions of cations with polar oxidic surfaces.[32] Moreover, a general enrichment of glycine and alanine in the tyrosine-containing sequences is evident. These residues generally offer increased conformational freedom to the peptide. It might be

dx.doi.org/10.1021/ja505413e | J. Am. Chem. Soc. 2014, 136, 12667−12674

straightforward to speculate that this can contribute to the ease of enzymatic modification and/or optimized positioning of functionalities for surface contacts. Interestingly, the enriched types of amino acid residues are also more prominent in common motifs of mussel adhesive proteins. Sequences of mefp-3 and mefp-5 apart from L-dopa are dominated by very few amino acids such as glycine and basic amino acids. The mefp-5 protein additionally contains a high amount of serine residues, which are mostly phosphorylated in the active protein state.[33−35] Therefore, the biocombinatorial phage display approach obviously selects analogues of amino acid compositions, which are also relevant for the biological adhesive systems.

A different selection of amino acids was found, when peptide sequences that contain no tyrosine were analyzed, indicating alternative interaction modes of peptide binders without L-dopa. Most obviously, basic amino acids show a cumulative increase of ∼11% if compared to the Tyr-bearing sequence set. This result was consistent with other biocombinatoric screenings on aluminum.[36] Proline and phenylalanine are slightly favored, whereas the other hydrophobic amino acids, including both glycine and alanine, are generally reduced.

From the pool of selected peptides, four different sequences have been chosen for further investigation (cf. Figure 2). Peptide-poly(ethylene oxide) conjugates (Pep-PEO) were synthesized to study enzyme substrate properties as well as adsorption/adhesion properties prior and after enzymatic processing. Two peptide sequences were chosen, which exhibit a seemingly important N-terminal tyrosine residue (Pep_1 and Pep_2). While Pep_1 was the only sequence containing three tyrosine residues and therefore might be the most promising adhesive, Pep_2 comprised the most abundant sequence found 21-times. Pep_3 was selected because it contains no N-terminal Tyr residue but one on sequence position 3. Moreover, Pep_3 shows on the one hand some sequence analogies to Pep_2 as Tyr^9 shares related neighbors. On the other hand, similarities of tyrosine positions and their neighbors to the well-studied mefp-1 repetitive sequence are evident (AKP<u>S</u>**Y**^{5}P<u>P</u><u>T</u>**Y**^{9}<u>K</u>; similar neighbors are underlined).[20] Furthermore, Pep_3 provides glycine, serine, histidine, and arginine. Hence, a relation to the composition of amino acids found in mussel adhesive protein mefp-5 is shown.[34,35] Finally, Pep_4 represents the reference sequence for a non-tyrosine containing adhesion domain for aluminum oxide. The peptide-poly(ethylene oxide) conjugates with PEO blocks of $M_{n,PEO}$ = 3200 were accessed via solid-phase supported synthesis by inverse conjugation strategies.[37] Prior work indicated that adhesion properties of peptide-PEO conjugates can be studied in comparison to non-conjugated peptides in a more accurate manner due to suppression of multilayer formation.[28]

UV−vis activation assays were carried out in order to investigate the substrate characteristics for each of the tyrosine containing conjugates. For this purpose, solutions of the different bioconjugates in pH 6.5 potassium phosphate buffer were oxidized by 100 u/mL tyrosinase in the presence of ascorbic acid (70 μM). As the absorbance maximum of L-dopa is at 280 nm, enzymatic oxidation of tyrosine over time can be monitored at that wavelength (Figure 3).[29] Noteworthy, due to the UV absorbance of ascorbic acid, its applied concentration during UV kinetics cannot be sufficiently high to keep tyrosine oxidation in the L-dopa state over 8h. Therefore, in the UV kinetics oxidation to the corresponding dopa-quinone-derivate is observed.

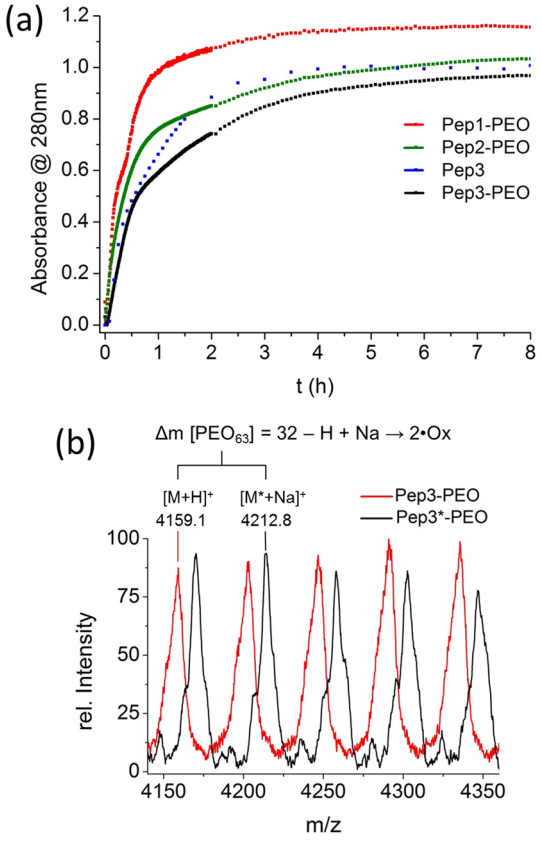

Figure 3. Enzymatic activation assays of Pep_3 and the $Pep_{(1-3)}$-PEO conjugates revealing distinct differences in oxidation kinetics by UV spectroscopy (a) and MALDI-TOF-MS spectra of non-activated Pep_3-PEO compared to L-dopa carrying activated Pep_3*-PEO (b). Conditions: (a) and (b): 0.29 mM conjugates in potassium phosphate buffer (pH 6.5), 100 u/mL enzyme, 25 °C; (a) 70 μM ascorbic acid, (b) 7 mM ascorbate, 8 h.

The kinetics indicate that all bioconjugates $Pep_{(1-3)}$-PEO have excellent tyrosinase substrate characteristics and oxidation levels off after approximately 2−4 h. MALDI-TOF-MS confirmed complete oxidation of both Pep_2-PEO and Pep_3-PEO (cf. SI, Figure S17 and S18). However, a quantitative oxidation of Pep_1-PEO under the applied conditions was not achieved. Mass spectrometry indicated a mixture of two and three oxidized tyrosines (cf. SI, Figure S16), which is consistent with the spectroscopic activity assay. Both Pep_2-PEO and Pep_3-PEO with two tyrosines result in a final absorbance of ∼1.0, whereas Pep_1-PEO containing three tyrosines reaches only ∼1.2. Noticeably, oxidation kinetics of non-conjugated Pep_3 showed a rather similar progression compared to Pep_3-PEO, suggesting that the PEO-block does not dramatically influence the enzyme−substrate recognition as previously also reported for congener bioconjugates.[20] Quantification of dopa-content of the PEO-peptide conjugates under the applied conditions is not trivial. Nonetheless, incubation of the synthetic di-dopa containing analogue Pep_3*$^{\text{-synth.}}$-PEO with tyrosinase under the same conditions as compared to the kinetic oxidation experiments yielded a final absorbance of 0.99 ± 0.06 au at 280 nm (cf. SI). The absorption value meets the same absorption region reached by all activated bioconjugates, which contain 2 tyrosine residues. Hence, enzymatic activation of Pep_3, Pep_2-PEO, and Pep_3-PEO can be considered as practically quantitative. Enzymatic oxidation of Pep^1-PEO, which con-

dx.doi.org/10.1021/ja505413e | J. Am. Chem. Soc. 2014, 136, 12667−12674

tained 3 Tyr residues, resulted obviously in a product mixture. To exclude that the tyrosinase oxidation of peptides was not leading to the formation a peptide exhibiting the dioxidation product L-trihydroxyphenylalanine (2,4,5 or 3,4,5 isomer, L-topa) instead of two L-dopa residues, MS/MS studies were performed (cf. SI, Figure S50). The fragmentation products of the oxidized Pep_3 sequence show two L-dopa moieties and exclude the L-topa formation pathway to occur under the given conditions.

To confirm the switchability of the bioconjugate adhesive-function, proof of an enzyme-induced transition of the peptide segments from weak to strong binders is required. For that purpose, quartz crystal microbalance (QCM) measurements have been conducted, investigating the enzymatically activable adhesion systems. The QCM experiments were carried out on aluminum oxide coated sensors, studying the adsorption and stability of the different non-activated $Pep_{(1-3)}$-PEO precursors and the corresponding L-dopa carrying oxidation products. During bioconjugate activation for QCM adsorption studies, high amounts of ascorbate were used assuring the immediate and quantitative reduction of L-dopaquinone residues as the immediate oxidation intermediate to L-dopa.

QCM experiments were performed at pH 6.5, where the oxidation mixture could be used directly without enzyme removal. At pH 4, which was required for high selection pressure-phage display, fast adsorption of tyrosinase to the QCM substrates was obvious (data not shown). This was not relevant during biopanning as the enzyme was carefully removed after phage library activation. Clearly, non-activated $Pep_{(1-3)}$-PEO and activated $Pep_{(1-3)}$*-PEO bioconjugates were distinguishable in adsorption rates and reversibility (Figure 4). All precursor bioconjugates represent weak and reversible aluminum oxide binders as indicated by minor frequency shifts of the QCM sensor (7−8 Hz) and almost complete elution of the precursors from the surface upon rinsing with buffer (pH 6.5). After activation, however, the amounts of adhered materials significantly increased for all bioconjugates, proving the successful screening procedure to directly select peptides useful for enzyme activable coatings. The analysis of adsorption isotherms indicated distinct differences in the binding processes of the activated systems. Pep_3*-PEO proved to be most efficient in terms of adsorption, reaching 85% of surface coating within 2 min. Application of the Voigt model[38] results in a calculated layer thickness of approximately 6 nm, suggesting an extended mushroom-like conformation of the conjugate. Pep_1*-PEO and Pep_2*-PEO also lead to efficient coatings, though reaching maximum surface coverage in a slower manner (cf. Figure 4a). Interestingly, extensive washing steps with buffer lead only to minor removal of the bioconjugates, indicating a non-reversible coating under these conditions. More noteworthy, however, is the fact that all $Pep_{(1-3)}$*-PEO lead to a stable coating, even defying model seawater solutions such as high concentrations of NaCl (599 mM) and in case of Pep_3*-PEO also nine salts solution (cf. SI, Figure S31).[39,40] Control experiments exclude the interference of the enzyme with the coating process, as tyrosinase shows only minor, slow adsorption (cf. Figure 4). Furthermore, the comparison of enzyme activated Pep_3*-PEO with directly synthesized, enzyme free Pep_3*-synth.-PEO shows equivalent adsorption isotherms and thus suggests enzyme co-adsorption to be negligible (cf. SI, Figure S28 and S29).

Adhesion under seawater conditions represents one of the major challenges for both technical wet glues and bioinspired

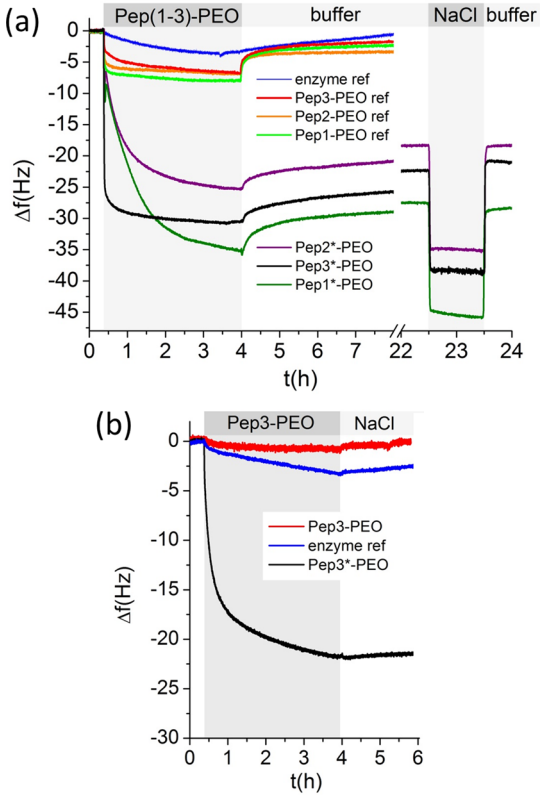

Figure 4. QCM adsorption and desorption kinetics of the set of bioconjugates in buffer (a) and under saltwater conditions (b). (a) Adsorption and desorption of non-activated conjugates $Pep_{(1-3)}$-PEO compared to activated $Pep_{(1-3)}$*-PEO conjugates. (b) Adsorption and desorption kinetics of non-activated Pep_3-PEO conjugate compared to the activated conjugate Pep_3*-PEO under saltwater conditions showing the effective generation of stable coatings in hostile environments. Conditions: (a) Buffer equilibrated aluminum oxide substrates were exposed to conjugate solutions and rinsed with 0.8 mM potassium phosphate buffer pH 6.5. The stability against saltwater was studied by rinsing the coatings with a solution of 599 mM NaCl, followed by buffer for end-point estimation and (b) solution of 599 mM NaCl.

coatings.[41,42] Hence, experiments were carried out under saltwater conditions, investigating the binding, adsorption, and desorption properties of Pep_3*-PEO as the most promising candidate. Figure 4 provides the QCM adsorption kinetics in 599 mM aqueous NaCl solution, which represents an established model electrolyte for seawater adhesion experiments.[39] Under these harsh, high-salt conditions, the activated bioconjugate Pep_3*-PEO adhered effectively onto aluminum oxide surfaces, whereas both the nonactivated Pep_3-PEO conjugate and the enzyme reference show very slow binding originating from a small sticking probability, which corresponds to low adhesion (cf. Figure 4b).

Comparison of the adsorption isotherms of Pep_3*-PEO at high-salt conditions with those in buffer (Figure 4b versus 4a) revealed a slower adsorption in the presence of salt but the same final frequency shift of −21 Hz. Hence, for both electrolyte solutions (low- and high-salt), comparable amounts of Pep_3*-PEO have been adsorbed. Furthermore, reference experiments with the L-dopa-containing conjugate Y*GY*G-PEO were carried out by QCM under comparable conditions (cf. SI, Figure S25). Noteworthy, only minor and reversible adsorption occurred in this case. This underlines the need for a

dx.doi.org/10.1021/ja505413e | J. Am. Chem. Soc. 2014, 136, 12667−12674

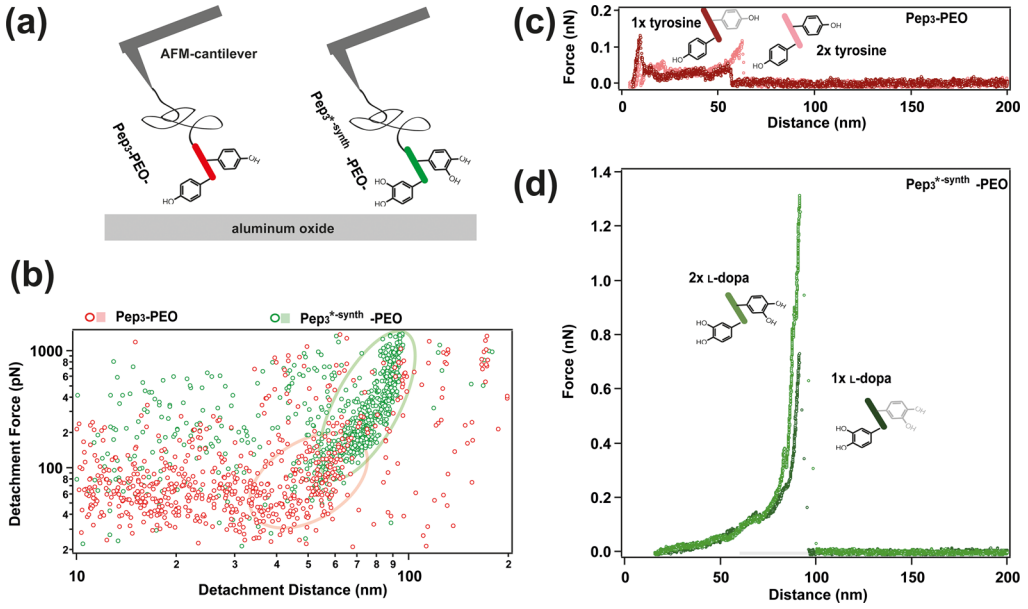

Figure 5. SMFS reveals differences in binding force between the activated (here synthesized, Pep_3*$^{-synth.}$) and the non-activated (Pep_3) domains on aluminum oxide surfaces and provides insights into interactions occurring on the molecular level. Schematic illustration of the measurement setup using a modified AFM-cantilever that bears a PEO-spacer with the non-activated (red) and activated peptides (green) Pep_3 and Pep_3*$^{-synth.}$, respectively (a). Scatter plots summarizing the forces required for the detachment of the adhesion domains from aluminum substrates in 0.8 mM potassium phosphate buffer (pH 6.7) together with the corresponding extension of the PEO-spacer (b). Exemplary force versus distance curves acquired with Pep_3-PEO-Probe and Pep_3*$^{-synth.}$-PEO-Probe (c, d). The large detachment forces for Pep $_3$*$^{-synth.}$-PEO-Probe can be attributed to one and two L-dopa moieties. By contrast, the forces for Pep_3-PEO-Probe correspond to interaction strengths expected for tyrosine.

more complex peptide sequence to compose multiple soft-interaction modes and mediate adhesion of binding L-dopa residues onto the target surface particularly under harsh conditions. Apparently, serine and arginine/histidine as common residues in adhesive domains significantly contribute to the Pep_3* adhesion processes, particularly under high-salt conditions. To show the binding effects of amino acids apart from L-dopa, NMR techniques are currently used that might offer insights into molecular binding events (results will be reported elsewhere). Additionally, the frequency shifts for the plateaus in the Langmuir isotherms were used to determine the binding constants of Pep_3*-PEO (cf. SI, Figure S46).[43] Under buffered conditions, an association saturation constant for Pep_3*-PEO of $K_A = 1.63 \pm 0.32 \times 10^6$ M^{-1} has been determined, categorizing the L-dopa bearing bioconjugate as a very strong binder for aluminum oxide.[24] Even more important were binding constants for the activable system under saltwater conditions. Whereas non-activated Pep_3-PEO did not show adsorption even at higher concentrations, for Pep_3*-PEO a $K_{A,NaCl} = 4.00 \pm 0.70 \times 10^4$ M^{-1} could be calculated (cf. SI). As could be expected, the binding constant of the activated bioconjugate decreases in high ionic strength medium. However, the adhesive still shows remarkably high affinity toward aluminum oxide under these harsh conditions.

The adhesion of *de novo* 12-mer peptides can be probed by single molecule force spectroscopy (SMFS) based on the atomic force microscopy (AFM) in order to provide a more quantitative insight into the binding process on the molecular level. In the SMFS experiments the adhesion of the most promising candidate Pep_3 onto aluminum oxide was studied. For that purpose, Pep_3 and chemically (enzyme free) synthesized Pep_3*$^{-synth.}$ were covalently coupled by Cys-maleimide ligation to a PEO-spacer that was attached on the other chain end to an amino-silane modified AFM-tip (Figure 5a and SI Figure S47).[44] The PEO-spacer and the peptide span a maximum length of approximately 110 nm in a fully extended, all-trans conformation. The SMFS measurements enable the comparison of the difference in adhesion for non-oxidized Pep_3-PEO-Probes and Pep_3*$^{-synth.}$-PEO-Probes on aluminum oxide surfaces. A significant difference of binding strength between non-oxidized and oxidized peptide segments was observed and therefore confirmed the QCM findings. Exemplary, force−distance curves for Pep_3-PEO-Probes and Pep_3*$^{-synth.}$-PEO-Probes are shown in Figure 5 (cf. c,d). Detachment events have been observed in about 35% and 20% of the force curves for Pep_3*$^{-synth.}$-PEO-Probe and Pep_3-PEO-Probe, respectively. A scatter plot provides a summary of the detachment forces and related PEO-extension lengths for all unbinding events of peptides from the surface (cf. Figure 5b). Clearly, the two peptides differ in the detachment forces and the corresponding extension lengths of the PEO-spacers. Whereas detachment of Pep_3-PEO-Probes occurs generally at much lower forces and smaller separation lengths of 30−60 nm, Pep_3*$^{-synth.}$-PEO-Probe detachment occurs at larger forces and significantly longer distances of 60−100 nm. This difference was expected, as stronger surface binding of the activated peptide segment enables an extended stretching of the PEO-spacer before detachment occurs.

A quantitative evaluation provides insight into the forces acting on the molecular level. The unbinding forces for detachments are obtained for a selected set of PEO-peptide conjugates that have been identified by statistical means from a large number of force curves (cf. SI). A bimodal distribution with remarkably high unbinding forces for Pep_3*$^{-synth.}$-PEO-Probes of 640 ± 140 and 1160 ± 390 pN, respectively, per activated peptide was observed. The latter detachment force is in the same order of magnitude as the force of 1.4 ± 0.3 nN necessary to rupture Au−S bonds,[45] but slightly too small to

dx.doi.org/10.1021/ja505413e | J. Am. Chem. Soc. 2014, 136, 12667−12674

challenge a C−C bond with 2.6 nN.[46] On the other hand, non-activated Pep_3-PEO-Probes show with about 55 ± 25 and 100 ± 25 pN a much weaker binding to the surface. Hence, Pep_3* clearly leads to a very strong non-covalent binding. The interesting bimodality in the detachment forces for both peptides can be rationalized by the fact that the adhesive peptides exhibit two binding loci, e.g. Pep_3*$^{\text{-synth.}}$-PEO-Probe bears two L-dopa residues enabling surface attachment via either both or only one L-dopa. Single molecule force spectroscopy enables tracing those binding events in the force curves (cf. Figure 5 c,d). These lower detachment forces for the peptides are in good agreement with the values reported by Messersmith et al. for L-tyrosine and L-dopa binders on oxidic surfaces.[47] Furthermore, the detachment of Pep_3*$^{\text{-synth.}}$-PEO and Pep_3-PEO as measured by SMFS is consistent with the binding behavior observed by QCM. Hence, the single molecule experiments suggest the origins of strong binding to be primarily mediated by L-dopa, confirming the importance of tyrosine for the activable adhesion systems.

The strong binding of Pep_3*-PEO to aluminum oxide surfaces subsequently subsequently enables the preparation of "PEGylated" surfaces, which could suppress interactions with proteins and are of great interest for biomedical applications due to anti-fouling characteristics. QCM experiments were performed to study the adsorption of model proteins onto Pep_3*-PEO coatings. Comparison of non-coated and coated aluminum oxide surfaces reveals significant reduction of protein adsorption. The latter coating results in an almost fully reversible protein adsorption. For instance, where bovine serum albumin (BSA) adsorbs strongly and irreversibly onto non-coated aluminum oxide leading to frequency shifts of about −35 Hz, Pep_3*-PEO coated surfaces reduced the amount of adsorbed BSA by 72% (Figure 6a). A more effective coating was generated when adhesion of Pep_3*-PEO was carried out closer to the PEO cloud point at 55 °C.[48] These more compact coatings completely defy BSA, leading to fully reversible adsorption (Figure 6a). However, treatment of coatings with fetal bovine serum or human full blood serum seems to be more relevant for practical applications (cf. Figure 6b and SI). Pep_3*-PEO coated surfaces resist both protein cocktails, as sensor frequencies practically return to initial values upon buffer rinsing. Instead, non-coated Al_2O_3 surfaces show high and irreversible serum adsorption. Furthermore, on the non-coated surface adsorbed human serum proteins even precipitate upon rinsing with Millipore water, which can be suggested from the short frequency drop, while dissipation shows a fast formation of a rather rigid layer (c.f. SI, Figure S37). In comparison, adsorption of serum proteins could be significantly reduced by 95%. Thereby, anti-fouling properties of non-covalent Pep_3*-PEO coatings show similar effects in the range of covalent aluminum coatings with comparable PEO layer thickness.[49] This low adsorption not only shows a sufficiently dense coating of PEO on the surface but also highlights the binding strength of Pep_3*-PEO on aluminum oxide, as displacement by proteins is negligible.

■ CONCLUSIONS

In conclusion, the integration of an enzymatic processing step into phage display biopanning enabled the direct selection of 12-mer peptides, which serve as excellent *de novo* substrates for tyrosinase. As implemented by the screening conditions, the native non-oxidized peptides show weak binding properties to aluminum surfaces but switch toward high-strength binders

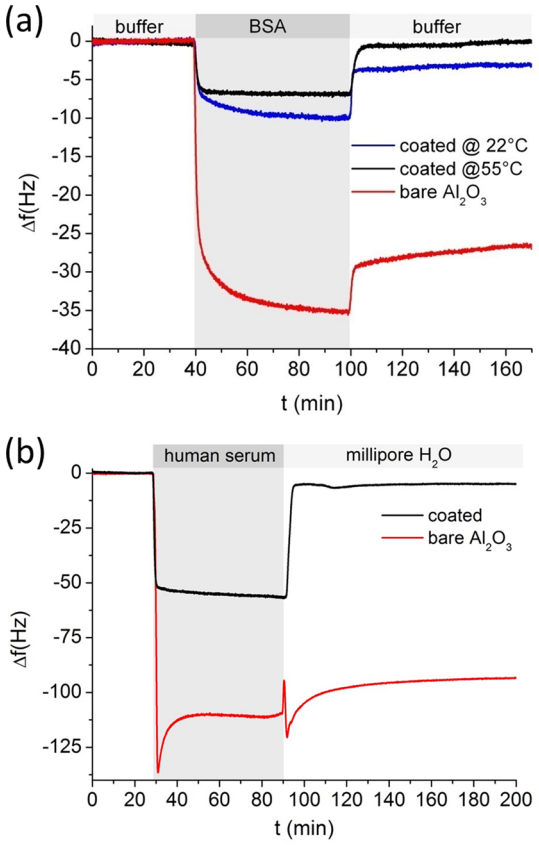

Figure 6. QCM experiments demonstrating the anti-fouling properties of Pep_3*-PEO coated aluminum compared to non-coated aluminum oxide surfaces. (a) Kinetics and reversibility of BSA adsorption onto Pep_3*-PEO coatings (coating @ 22 and 55 °C) revealing near cloud point coatings to be most efficient. (b) Adsorption isotherms demonstrating the reversibility of the adsorption of human serum protein cocktails on Pep_3*-PEO coated aluminum (coating @ 55 °C compared to non-coated aluminum).

after being oxidized by tyrosinase. Measurements of the adsorption kinetics for resulting peptide-*block*-poly(ethylene oxide) bioconjugates (Pep-PEO) in non-activated and activated state highlight dramatic changes in the adsorption rates, adsorption constants, and reversibility of adsorption upon rinsing. Noticeably, all coatings of the activated bioconjugates (Pep*-PEO) withstood intense washing with model seawater solutions. The most promising candidate was HSY*SGW-SPY*RSG-*block*-PEO (Pep_3*-PEO, where Y* equals L-dopa) as adherence took place effectively even under high-salt conditions. SMFS quantified the dramatic differences in adhesion for Pep_3-PEO (nonactivated) and Pep_3*$^{\text{-synth}}$-PEO (activated), revealing a maximum difference in binding forces per peptide molecule by a factor of approximately 10. Langmuir adsorption isotherms indicated for Pep_3*-PEO binding constants of $K_A = 1.63 \times 10^6\ M^{-1}$, categorizing the oxidized adhesion domain as a very strong binder. The resulting coatings exhibited anti-fouling properties, as adsorption of BSA proteins and full blood serum was strongly reduced and practically reversible upon washing. The directed selection of *de novo* adhesive peptides via extended phage display biopanning enabled one to realize tyrosinase activated adhesives showing a transition from weak to strong binders. Extended phage display screening offers direct access to enzymatically processable non-natural peptide domains. The study demon-

dx.doi.org/10.1021/ja505413e | J. Am. Chem. Soc. 2014, 136, 12667−12674

strated the identification of activable adhesion domains and provides further insight into the concerted process of complex bioadhesion. However, the process is more generic and might pave the way toward the general screening for suitable substrates for a large variety of posttranslational modifications.

■ ASSOCIATED CONTENT

Supporting Information

Materials; methods; phage display data; NMR, IR, MALDI, and HPLC results for synthesized substances; MALDI of activated peptides/conjugates; QCM experiments under various conditions; SMFS data evaluation. This material is available free of charge via the Internet at http://pubs.acs.org.

■ AUTHOR INFORMATION

Corresponding Author

h.boerner@hu-berlin.de

Notes

The authors declare no competing financial interest.

■ ACKNOWLEDGMENTS

The authors acknowledge Dr. S. Weidner (BAM-Berlin) for enabling access to the MALDI-TOF-MS instrument, Dr. E. Krause (FMP Berlin) for the NanoLC-MS/MS analytic, K. Linkert (HU Berlin) for synthesis of control peptides, and T. Schwemmer (HU Berlin) and J. Baumgartner (MPIKG, Potsdam) for introduction to phage display. H.G.B. and D.F. would like to acknowledge financial support by the German research council (DFG BEKs BO1762/5-1). Further support was granted for HGB by the European Research Council under the European Union's 7th Framework Program (FP07-13)/ERC starting grant "Specifically Interacting Polymer−SIP" (ERC 305064). This research was supported in DF's lab by the Max Planck Society and a starting Grant from the European Research Council (Project MB2, no. 256915). G.P. acknowledges support by the German research council (SFB 840).

■ REFERENCES

(1) Lee, H.; Lee, B. P.; Messersmith, P. B. *Nature* **2007**, *448*, 338.
(2) Lee, B. P.; Messersmith, P. B.; Israelachvili, J. N.; Waite, J. H. *Annu. Rev. Mater. Res.* **2011**, *41*, 99.
(3) Waite, J. H.; Tanzer, M. L. *Science* **1981**, *212*, 1038.
(4) Lee, H.; Dellatore, S. M.; Miller, W. M.; Messersmith, P. B. *Science* **2007**, *318*, 426.
(5) Lin, Q.; Gourdon, D.; Sun, C. J.; Holten-Andersen, N.; Anderson, T. H.; Waite, J. H.; Israelachvili, J. N. *Proc. Natl. Acad. Sci. U. S. A.* **2007**, *104*, 3782.
(6) Deming, T. J. *Curr. Opin. Chem. Biol.* **1999**, *3*, 100.
(7) Brubaker, C. E.; Messersmith, P. B. *Langmuir* **2012**, *28*, 2200.
(8) Waite, J. H.; Housley, T. J.; Tanzer, M. L. *Biochemistry* **1985**, *24*, 5010.
(9) Hwang, D. S.; Zeng, H. B.; Masic, A.; Harrington, M. J.; Israelachvili, J. N.; Waite, J. H. *J. Biol. Chem.* **2010**, *285*, 25850.
(10) Burzio, L. A.; Waite, J. H. *Biochemistry* **2000**, *39*, 11147.
(11) Messersmith, P. B. *Science* **2008**, *319*, 1767.
(12) Yu, M. E.; Hwang, J. Y.; Deming, T. J. *J. Am. Chem. Soc.* **1999**, *121*, 5825.
(13) Harrington, M. J.; Masic, A.; Holten-Andersen, N.; Waite, J. H.; Fratzl, P. *Science* **2010**, *328*, 216.
(14) Yamamoto, H.; Hayakawa, T. *Polymer* **1978**, *19*, 1115.
(15) Su, J.; Chen, F.; Cryns, V. L.; Messersmith, P. B. *J. Am. Chem. Soc.* **2011**, *133*, 11850.
(16) Black, K. C. L.; Yi, J.; Rivera, J. G.; Zelasko-Leon, D. C.; Messersmith, P. B. *Nanomedicine* **2013**, *8*, 17.
(17) Dalsin, J. L.; Hu, B. H.; Lee, B. P.; Messersmith, P. B. *J. Am. Chem. Soc.* **2003**, *125*, 4253.
(18) Holten-Andersen, N.; Harrington, M. J.; Birkedal, H.; Lee, B. P.; Messersmith, P. B.; Lee, K. Y. C.; Waite, J. H. *Proc. Natl. Acad. Sci. U.S.A.* **2011**, *108*, 2651.
(19) Yu, M. E.; Deming, T. J. *Macromolecules* **1998**, *31*, 4739.
(20) Wilke, P.; Boerner, H. G. *ACS Macro Lett.* **2012**, *1*, 871.
(21) Smothers, J. F.; Henikoff, S.; Carter, P. *Science* **2002**, *298*, 621.
(22) Douglas, T.; Young, M. *Science* **2006**, *312*, 873.
(23) Whaley, S. R.; English, D. S.; Hu, E. L.; Barbara, P. F.; Belcher, A. M. *Nature* **2000**, *405*, 665.
(24) Serizawa, T.; Matsuno, H.; Sawada, T. *J. Mater. Chem.* **2011**, *21*, 10252.
(25) Baumgartner, J.; Carillo, M. A.; Eckes, K. M.; Werner, P.; Faivre, D. *Langmuir* **2014**, *30*, 2129.
(26) Gebauer, D.; Verch, A.; Boerner, H. G.; Coelfen, H. *Cryst. Growth Des.* **2009**, *9*, 2398.
(27) Sarikaya, M.; Tamerler, C.; Jen, A. K. Y.; Schulten, K.; Baneyx, F. *Nat. Mater.* **2003**, *2*, 577.
(28) Schwemmer, T.; Baumgartner, J.; Faivre, D.; Boerner, H. G. *J. Am. Chem. Soc.* **2012**, *134*, 2385.
(29) Marumo, K.; Waite, J. H. *Biochim. Biophys. Acta* **1986**, *872*, 98.
(30) Zuo, R. J.; Ornek, D.; Wood, T. K. *Appl. Microbiol. Biotechnol.* **2005**, *68*, 505.
(31) Matos-Perez, C. R.; White, J. D.; Wilker, J. J. *J. Am. Chem. Soc.* **2012**, *134*, 9498.
(32) Vallee, A.; Humblot, V.; Pradier, C.-M. *Acc. Chem. Res.* **2010**, *43*, 1297.
(33) Papov, V. V.; Diamond, T. V.; Biemann, K.; Waite, J. H. *J. Biol. Chem.* **1995**, *270*, 20183.
(34) Hwang, D. S.; Yoo, H. J.; Jun, J. H.; Moon, W. K.; Cha, H. J. *Appl. Environ. Microbiol.* **2004**, *70*, 3352.
(35) Waite, J. H.; Qin, X. X. *Biochemistry* **2001**, *40*, 2887.
(36) Adams, B. L.; Finch, A. S.; Hurley, M. M.; Sarkes, D. A.; Stratis-Cullum, D. N. *Adv. Mater.* **2013**, *25*, 4585.
(37) Lutz, J.-F.; Börner, H. G. *Prog. Polym. Sci.* **2008**, *33*, 1.
(38) Hook, F.; Kasemo, B.; Nylander, T.; Fant, C.; Sott, K.; Elwing, H. *Anal. Chem.* **2001**, *73*, 5796.
(39) Sharqawy, M. H.; Lienhard, J. H.; Zubair, S. M. *Desalin. Water Treat.* **2010**, *29*, 355.
(40) Marden, P.; Tunlid, A.; Malmcronafriberg, K.; Odham, G.; Kjelleberg, S. *Arch. Microbiol.* **1985**, *142*, 326.
(41) Stewart, R. J.; Ransom, T. C.; Hlady, V. *J. Polym. Sci., Part B* **2011**, *49*, 757.
(42) Rahman, M. M.; Lee, I.; Chun, H.-H.; Kim, H. D.; Park, H. *J. Appl. Polym. Sci.* **2014**, *131*, 39905.
(43) Wangchareansak, T.; Sangma, C.; Ngernmeesri, P.; Thitithanyanont, A.; Lieberzeit, P. A. *Anal. Bioanal. Chem.* **2013**, *405*, 6471.
(44) Ebner, A.; Wildling, L.; Zhu, R.; Rankl, C.; Haselgruebler, T.; Hinterdorfer, P.; Gruber, H. J. In *STM and AFM Studies on (Bio) molecular Systems: Unravelling the Nanoworld*; Samori, P., Ed.; Springer-Verlag: Berlin, 2008; p 29.
(45) Grandbois, M.; Beyer, M.; Rief, M.; Clausen-Schaumann, H.; Gaub, H. E. *Science* **1999**, *283*, 1727.
(46) Sheiko, S. S.; Sun, F. C.; Randall, A.; Shirvanyants, D.; Rubinstein, M.; Lee, H.; Matyjaszewski, K. *Nature* **2006**, *440*, 191.
(47) Lee, H.; Scherer, N. F.; Messersmith, P. B. *Proc. Natl. Acad. Sci. U.S.A.* **2006**, *103*, 12999.
(48) Kingshott, P.; Thissen, H.; Griesser, H. J. *Biomaterials* **2002**, *23*, 2043.
(49) Weber, T.; Bechthold, M.; Winkler, T.; Dauselt, J.; Terfort, A. *Colloids Surf., B* **2013**, *111*, 360.